

Magnéli-Phases in Anatase Strongly Promote Co-Catalyst-Free Photocatalytic Hydrogen Evolution

Maximilian Domaschke,^{#a} Xuemei Zhou,^{#b} Lukas Wergen,^a Stefan Romeis,^a

*Matthias E. Miehlich,^c Karsten Meyer,^c Wolfgang Peukert,^{*a} Patrik Schmuki^{*b}*

a. Institute of Particle Technology, University of Erlangen-Nuremberg, Cauerstr. 4, 91058 Erlangen, Germany.

b. Department of Materials Science WW-4 LKO, University of Erlangen-Nuremberg, Martensstr. 7, 91058 Erlangen, Germany.

c. Department of Chemistry and Pharmacy, Inorganic & General Chemistry, University of Erlangen-Nuremberg, Egerlandstrasse 1, 91058 Erlangen, Germany.

Link to the published article:

<https://pubs.acs.org/doi/abs/10.1021/acscatal.9b00578>

ABSTRACT

Magnéli phases of titanium dioxide (such as Ti_4O_7 , Ti_5O_9 , etc.) provide electronic properties, namely a stable metallic behavior at room temperature. In this manuscript, we demonstrate that nanoscopic Magnéli phases, formed intrinsically in anatase during a thermal aerosol synthesis, can enable significant photocatalytic H_2 generation – this without the use of any extrinsic co-catalyst in anatase. Under optimized conditions, mixed phase particles of 30% anatase, 25% Ti_4O_7 and 20% Ti_5O_9 are obtained that can provide, under solar light, direct photocatalytic H_2 evolution at a rate of $145 \mu\text{mol h}^{-1} \text{g}^{-1}$. These anatase particles contain 5-10 nm size inter-grown phases of Ti_4O_7 and Ti_5O_9 . Key is the metallic band of Ti_4O_7 that induces a particle internal charge separation and transfer cascade with suitable energetics and favorable dimensions that are highly effective for H_2 generation.

KEYWORDS: Magnéli phase, Photocatalysis, H_2 evolution, Titanium Sub-oxide, Anatase

Magnéli phases are a set of titanium sub-oxides with a general composition of $\text{Ti}_n\text{O}_{2n-1}$, where n varies from 3 to 10, such as Ti_4O_7 , Ti_5O_9 , etc. The structures of this specific set of titanium suboxides were described in the 1950s by Magnéli et al.¹⁻⁴ Typical synthesis routes involve carbothermal reduction,⁵ reducing rutile with CaH_2 at $350 \text{ }^\circ\text{C}$,⁶ or reducing anatase or rutile in hydrogen atmosphere at temperatures typically $>1200 \text{ }^\circ\text{C}$.⁷ The compounds have in common that they consist of distorted TiO_6 octahedra which are joined by sharing edges to form an infinite three-dimensional framework.⁶ The deviation from the ideal TiO_2 stoichiometry is accommodated for by oxygen vacancies regularly arranged throughout the lattice.⁸⁻¹¹ As a result, many Magnéli

phases provide an electronic structure that shows a metallic behavior at room temperatures.¹²⁻¹⁶ For example, for Ti_4O_7 the Fermi level at room temperature is located within the oxide's conduction band and the material has an electronic conductivity that is comparable to metals.¹⁷⁻¹⁹ Due to this feature, Magnéli phases are industrially used as conductive oxide electrodes that provide a wide electrochemical window, comparable or superior to graphite or lead.^{20, 21}

Interestingly, theoretical work also shows the filled metallic band of the Magnéli phases, namely Ti_4O_7 , to be located close to the conduction band edge of TiO_2 . This makes Magnéli phases interesting in microelectronics and in particular in memristic devices where semiconductor/metal switching is exploited.^{5, 7, 22-27} Nevertheless, such semiconductor/metal junctions are also of a high interest for photocatalysis, where efficient charge separation within a catalyst particle and transfer of the photoinduced charge carriers to the surrounding media dictates the efficiency of a photocatalyst. Also in the case of anatase TiO_2 - the most widely investigated economic and stable photocatalyst with an energetics that allows water oxidation and reduction - kinetic limitations of the reactions can be overcome by designing suitable electronic junctions or defect structures.^{28, 29} Energetic gradients in junctions can give charge carriers separation directionality and lower the kinetic surface barriers, as in the case of noble metal co-catalysts (Au, Pt, Pd) that are widely used, when H_2 generation from TiO_2 should be achieved at reasonable rates.

For the effectiveness of a particle internal junction it is of key importance that the dimensions are adjusted to the carrier diffusion/drift length. With a typical hole diffusion length in the range of some 10 nm in anatase³⁰, size and energy matching junction engineering is desired. For example Bahnemann et al. discuss a variety of critical processing factors that affect the H_2 evolution performance when anatase/rutile photocatalysts are formed by wet synthesis.³¹ Previous work also

used several reduction treatments to create low concentration Ti^{3+} -Ov states that were able to mediate electron transfer from anatase particles.³² In contrast in the present work, we use a H_2 stream thermal aerosol hot-wall reactor synthesis that is able to induce nanoscopic Magnéli phase segments into growing anatase nanocrystals. The synthesis is described in detail in the SI and allows to fabricate Ti_4O_7 and Ti_5O_9 containing TiO_2 nanoparticles with a narrow size distribution (particle size <100 nm) and with a variable ratio of anatase to Magnéli phase. We find these particles to exhibit the remarkable feature to strongly enhance photocatalytic H_2 generation without the use of any external co-catalyst.

Figure 1a shows XRD spectra for samples synthesized at different processing temperatures (from 500 °C to 1000 °C) and **Figure 1b** gives the evaluation of the phase composition of the powder. Rietveld analysis of the diffractograms shows that at temperatures of up to 500 °C only anatase is formed. At higher temperatures (800 °C), small amounts of Magnéli phase (< 5%) start to appear. For 900 °C, clear peaks for Ti_3O_5 (PDF No. 01-072-2101, Ti_3O_5 , Orthorhombic, Cmc \bar{m} space group), Ti_4O_7 (PDF No. 01-072-1724, Ti_4O_7 , Anorthic, A-1 space group), Ti_5O_9 (PDF No. 01-071-0627, Ti_5O_9 , Anorthic, P-1 space group) can be observed, with a phase composition of 30% anatase, 15% rutile and 55% Magnéli phase. At 1000 °C, Magnéli phases reach 60% Ti_4O_7 and 20% Ti_5O_9 and < 10% anatase and rutile are present. For samples prepared at 1100 °C, XRD shows Ti_4O_7 to be the main crystalline phase in the material with only < 5% anatase left. Importantly, **Figure S1** shows that our synthesis approach leads only to a slight increase of the particle size from 800 °C to 1100 °C, that is from approx. 22 nm at 800 °C to approx. 49 nm at 1100 °C.

Changes in the phase composition could be confirmed by Raman measurements (**Figure S4**). The inset in **Figure 1c** shows that the conversion to particles with an increased sub-oxide content

is also accompanied with a color change of the powder from white to dark blue. The samples maintain this appearance for several months at ambient conditions and at temperatures of up to 80 °C in air.

These powders were then investigated for their photocatalytic H₂ evolution activity under AM 1.5 (100 mW cm⁻²) solar simulator illumination and ultra violet light ($\lambda = 365$ nm, 90 mW cm⁻²), using suspensions of the particles in a H₂O/methanol solution. Please note that all experiments were performed without the use of noble metal co-catalyst (experimental details are given in the Supporting Information). The results in **Figure 1c** and **Figure S2** show that titania particles become increasingly active for H₂ evolution with increasing temperature under plain UV and solar irradiation up to 900 °C. An optimum activity is obtained for powder synthesized at 900 °C, a photocatalytic H₂ evolution rate of ≈ 145 $\mu\text{mol h}^{-1} \text{g}^{-1}$ is achieved.

For higher synthesis temperatures (>1000 °C), the materials show a diminishing activity, and for the sample prepared at 1100 °C, no H₂ evolution is detectable. This is in line with experiments performed with an untreated commercial Magnéli powder that was used for reference. It is noteworthy that a mild contribution from visible light to the overall H₂ production can be observed for the Magnéli-phase containing powder produced at 900 °C (**Figure S2b**). For this sample also repeated photocatalytic tests in cycling experiments (**Figure S2a**) show that the H₂ generation activity is stable over the investigated time interval of 24 h.

Figure 1d shows a high resolution HRTEM image of the most active sample, i.e. the sample prepared at 900 °C. The particle essentially consists of adjacent phases of Ti₄O₇ and anatase. The observed lattice fringes correspond to anatase [101] with a d spacing of 0.351 nm (i.e., corresponding to the XRD peak at $2\theta = 25.2^\circ$) and a spacing for Ti₄O₇ of 0.331 nm, which

corresponds to the [120] facet of Ti_4O_7 . I.e., the most active sample consists essentially of intergrown phases of anatase and Ti_4O_7 with similar domain sizes of 5-10 nm (the entire particle is approx. 30 nm in diameter). Also, from the SAED pattern the typical features of anatase and Ti_4O_7 can be identified but additionally traces of rutile [111] can be identified (**Figure 1d**). HRTEM images for a sample synthesized at 1000 °C (**Figure S3**) shows lattice spacings of 0.260 nm, 0.409 nm and 0.246 nm, which can be ascribed to the [200] facet of Ti_4O_7 , the [102] facet of Ti_5O_9 and the [121] of Ti_5O_9 and [120] of Ti_4O_7 . This is in line with XRD that indicate that the sample prepared at 1000 °C contains only 5% anatase, 20% Ti_5O_9 and 60% Ti_4O_7 .

X-ray photoelectron spectroscopy (XPS) data are shown in **Figure 2a** for the O1s peaks and in **Figure 2b** for the Ti2p peaks of samples prepared at 500 °C, 900 °C and 1100 °C. The O1s peak can be deconvoluted into three contributing peaks. The main peak at 529.6 eV corresponds to oxygen in the TiO_2 position. This peak intensity decreases with higher synthesis temperature (from 75.3% at 500 °C to 48.1% at 1100 °C). The peak at 531.9 eV can be attributed to defective oxygen species from Magnéli phase as described in literature^{6, 33, 34} and further confirmed by spectra taken on reference commercial Ti_4O_7 (**Figure S5**). This peak increases from 19.0% at 500 °C to 34.0% at 1100 °C.

The concentration at 1100 °C of 34.0% is well in line with the reference Ti_4O_7 (**Figure S5**), where a contribution of 36.3% of this peak to the overall spectrum is obtained. The peak at higher binding energy (533.6 eV) can be ascribed to surface adsorbed water.³⁵ The Ti2p peak for commercial Magnéli phase (**Figure S5**) shows two clear peaks at a binding energy of 456.0 eV and 461.7 eV, which can be attributed to titanium in nonstoichiometric TiO_2 .³⁶ The Ti2p peaks for sample prepared at 1100 °C (**Figure 2b**) shows only a mild sub-stoichiometry contribution, which

may be ascribed to the remaining anatase in the powder. However, overall, these findings are well in line with the formation of sub-oxides in the TiO_2 as well as the commercial Magnéli phase.³⁷

Figure 2c shows CW X-band EPR spectra for samples prepared in a temperature range from 500 °C to 1100 °C recorded at 100 K. The spectrum of the pure anatase (sample prepared at 500 °C), shows trace amounts of characteristic intrinsic defects (“F-centers” or oxygen vacancies in anatase³⁸) at $g \approx 2.0$. For samples synthesized at high temperature (800 °C to 1100 °C), and where XRD indicates the presence of a Magnéli phase, a broader and significantly more intense signal is apparent with a g -values ranging from 1.95-1.96. Compared with the EPR spectra of commercially available Magnéli crystallites (**Figure S6**) and literature data,³⁴ this signal is attributed to a $(\text{Ti}^{3+}\text{V}_\text{o}-\text{Ti}^{4+})^{+1}$ center, which consists of an electron localized on or about an oxygen vacancy with a possible charge transfer between the two Ti sites.³⁹

To obtain information on the electronic properties of the Magnéli phase containing samples, we carried out photoelectrochemical measurements as shown in **Figure 3a** and **Figure 3b**. Photocurrent spectra were taken from powder film samples on FTO for samples prepared at 500 °C, 800 °C, 900 °C and 1100 °C, and a commercial Magnéli phase pellet in 0.1 M Na_2SO_4 (see SI for details).

Figure 3a shows that with the increase of synthesis temperature, a decrease of the magnitude of the photocurrent in the UV is observed. The sample prepared at 1100 °C shows the clearly lowest photocurrent response but a very noticeable tail into the visible region. The band gap evaluation in **Figure 3b** gives a value of 3.21 eV for sample prepared at 500 °C, which corresponds well with values for the indirect band gap of anatase. However, for samples prepared at 800 °C and 900 °C, the band gap evaluation leads to an increasingly lower value of 3.15 eV for 800 °C 3.00 eV for

900 °C. This shift can be ascribed to the increasing contribution of sub-oxide species with occupied states close to the conduction band of anatase.^{40, 41}

To explain the beneficial effect of an anatase/Ti₄O₇ junction on the photocatalytic hydrogen generation one may consider previous theoretical work on the electronic structure of Magnéli phases and namely Ti₄O₇.^{37, 41} At room temperature, DOS calculations for Ti₄O₇ show a metallic band of a width of approx. 0.5 eV that consists of 3d Ti states with a formal Ti^{+3.5} charge. The electron hopping activation energies to move an electron from a Ti³⁺ to a neighboring Ti⁴⁺ is < 0.2 eV (i.e. sufficient to provide room temperature conductivity). The Fermi level of this metallic band, in absolute energy, is located approx. 0.1 – 0.2 eV below the conduction band of anatase. The energetic situation of an anatase/Ti₄O₇ junction can thus roughly be outlined as shown in **Figure 3c**. From these considerations, one can deduce Ti₄O₇ to act as a charge transfer mediator for photogenerated electrons (similar to a noble metal co-catalyst). Anatase, to a large extent, acts as the carrier harvesting phase whereas the Ti₄O₇ extracts electrons and mediates their transfer to the surrounding liquid phase. Due to the close proximity of anatase and Magnéli phase (in a single particle), charge carrier separation can be very efficient. Additionally, the Magnéli phase provides a high electronic conductivity, which ensures a high carrier mobility through the co-catalyst and thus further facilitates the charge separation in the photocatalytic process.

In conclusion, the present work shows that nanoscopic inserts of Magnéli phases, formed directly during anatase titania nanoparticle synthesis, can act as efficient co-catalyst in anatase for photocatalytic H₂ generation. For particle sizes <100 nm, anatase/Ti₄O₇ internal junctions are highly beneficial for charge separation, as with a size of ≈ 5-10 nm, the junction dimensions lie within the diffusion length of holes in anatase.⁴² Mixed phase particles of 30% anatase, 25% Ti₄O₇ and 20% Ti₅O₉ show the highest photocatalytic H₂ evolution activity (145 μmol h⁻¹ g⁻¹), without

the use of any extrinsic co-catalyst. Pure anatase or pure Magnéli phase yield significantly weaker photocatalytic H_2 generation activity. We attribute the enhanced photocatalytic performance of these mixed particles to the electronic properties of the Magnéli phases, where anatase acts as light harvester and Ti_4O_7 acts as mediator for charge separation, as well as for electron transport and transfer.⁴³ Furthermore, the synthesis approach used here allows for a wide in-situ variation of features, such as doping and decoration, and provides a potent tool for further direct modification of Magnéli/anatase based photocatalysts.

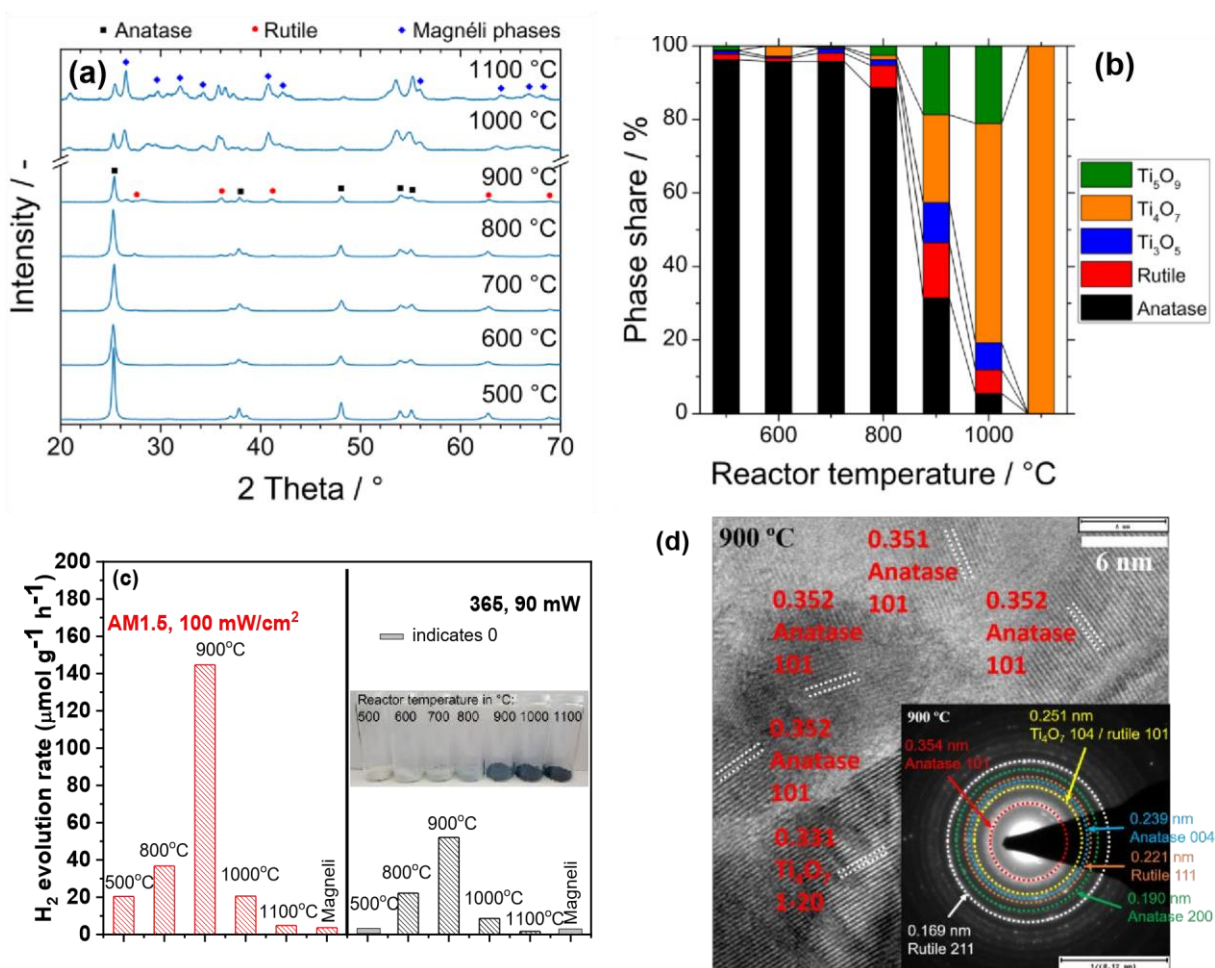


Figure 1. (a) XRD patterns for the as-synthesized materials. (b) Phase composition analysis based on **Figure 1a**. (c) Photocatalytic H_2 evolution from different phase coupled titania corresponding

to Figure 1a under 365 nm LED or AM1.5 (100 mW cm^{-2}) solar simulator illumination measured in a 50 vol% methanol–water electrolyte. Inset: optical images of the samples. (d). HRTEM images for sample prepared at 900 °C. Inset: SAED pattern and its analysis for the sample with maximum H_2 evolution activity (prepared at 900 °C.)

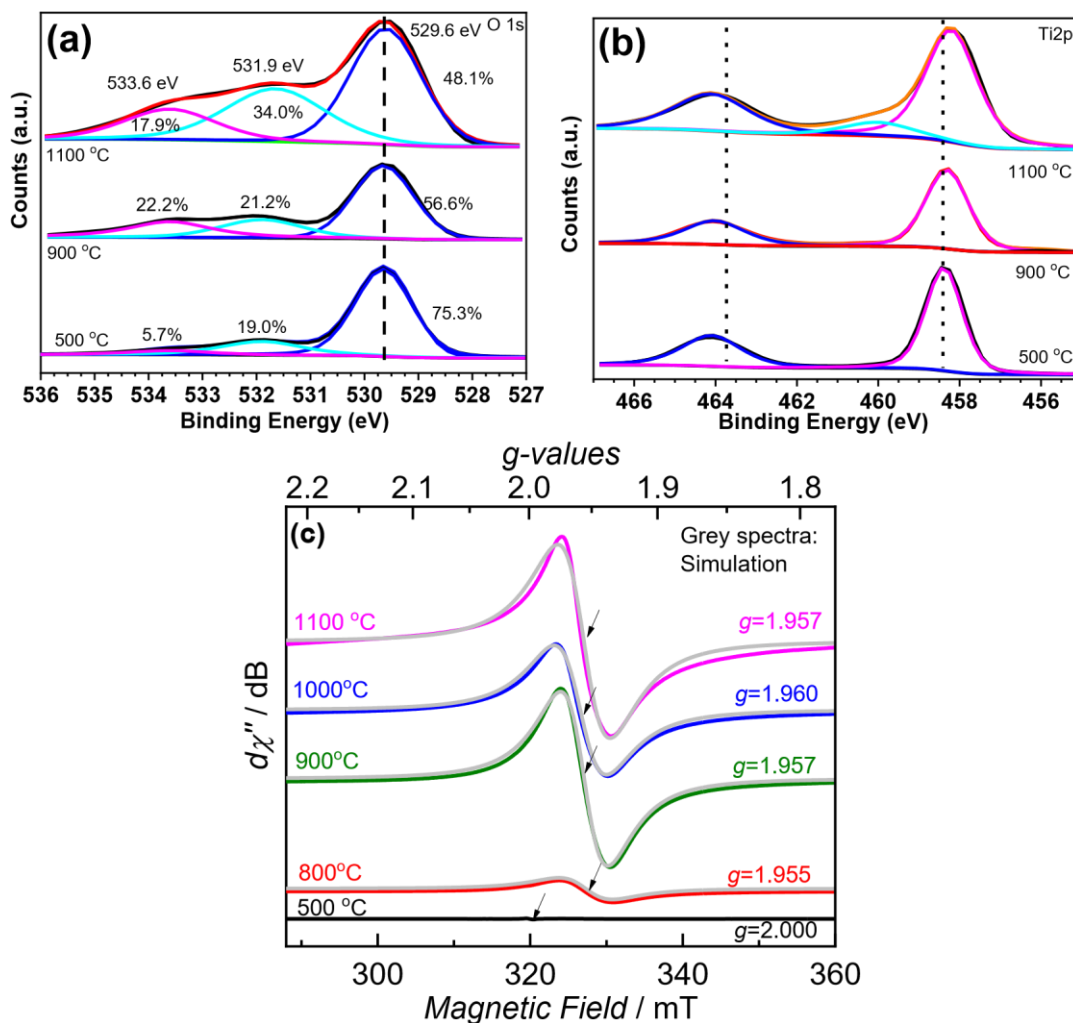


Figure 2. High resolution XPS (a) Ti2p and (b) O1s peaks for samples prepared at 500 °C, 900 °C and 1100 °C. (c) Solid-state EPR spectra for materials prepared from 500 °C to 1100 °C, measured at 100 K.

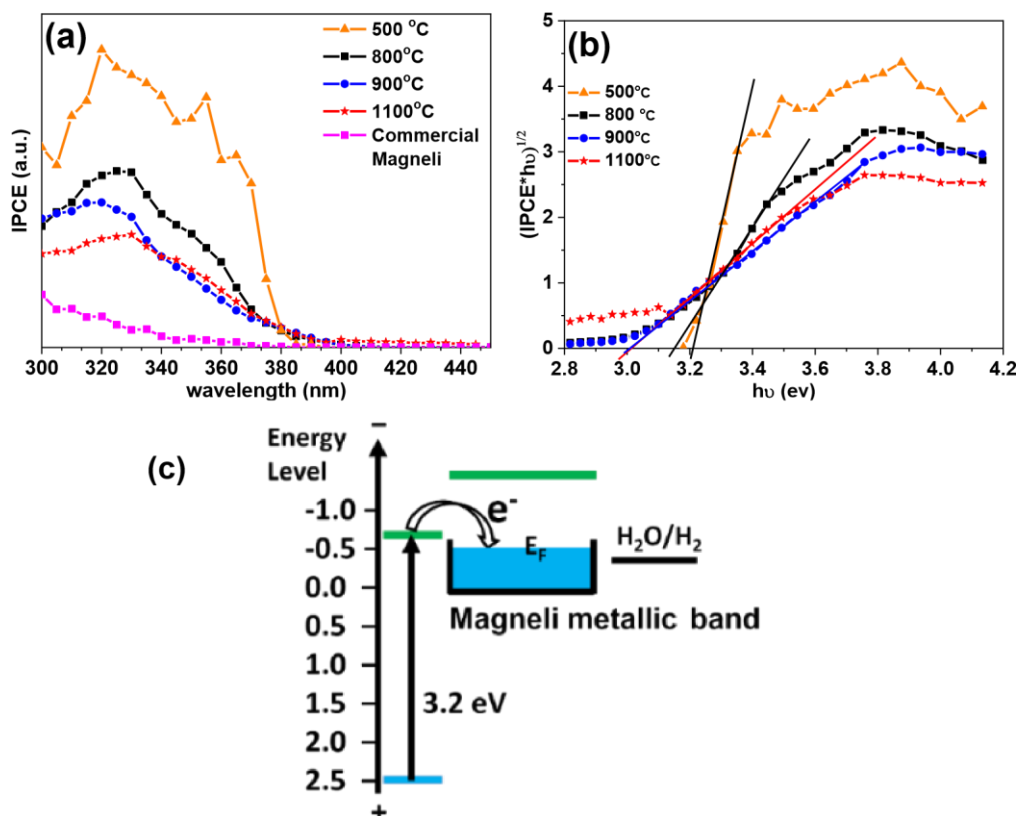


Figure 3 (a) Incident photocurrent conversion efficiency (IPCE) measurements for the as-synthesized materials as electrodes and (b) band gap evaluation from spectra in (a). (c) Schematic drawing for the band alignment between TiO₂ and Magnéli phase based on theory.

Corresponding Author

Wolfgang Peukert: E-mail: wolfgang.peukert@fau.de;

Patrik Schmuki: E-mail: schmuki@ww.uni-erlangen.de.

Author Contributions

The manuscript was written through contributions of all authors. All authors have given approval to the final version of the manuscript. # indicates equal contribution of the work by the authors.

Conflicts of interest

There are no conflicts to declare.

Supporting Information

Supporting Information include experimental section, SEM images of particles, stability tests of photocatalytic activity, Raman spectra, TEM images, XPS peaks and EPR of commercial Magnéli powder.

Acknowledgement

Financial support from ERC and DFG within the framework of its Excellence Initiative for the Cluster of Excellence “Engineering of Advanced Materials” is thankfully acknowledged.

REFERENCES

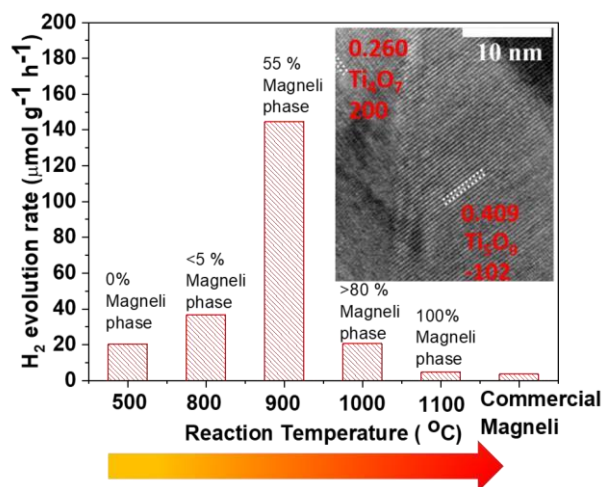
1. Andersson, S., The Crystal Structure of Ti_5O_9 . *Acta Chem. Scand.* **1960**, *14*, 1161-1172.
2. Åsbrink, S.; Magnéli, A., MagnéliCrystal Structure Studies on Trititanium Pentoxide, Ti_3O_5 . *Acta Cryst.* **1959**, *12*, 575-581.
3. Andersson, S.; Collen, B.; Kuylenstierna, U.; Magnéli, A., Phase Analysis Studies on the Titanium-Oxygen System. *Acta Chem. Scand.* **1957**, *11*, 1641-1652.
4. Andersson, S.; Collen, B.; Kruuse, G.; Kuylenstierna, U.; Magnéli, A.; Pestmalis, H.; Åsbrink, S., Identification of Titanium Oxides by X-Ray Powder Patterns. *Acta Chem. Scand.* **1957**, *11*, 1653-1657.
5. Wei, H.; Rodriguez, E. F.; Best, A. S.; Hollenkamp, A. F.; Chen, D.; Caruso, R. A., Chemical Bonding and Physical Trapping of Sulfur in Mesoporous Magneli Ti_4O_7 Microspheres for HighPerformance Li-S Battery. *Adv. Energy Mater.* **2017**, *7*, 1601616.
6. Tominaka, S.; Tsujimoto, Y.; Matsushita, Y.; Yamaura, K., Synthesis of Nanostructured Reduced Titanium Oxide: Crystal Structure Transformation Maintaining Nanomorphology. *Angew. Chem. Int. Ed.* **2011**, *50*, 7418-7421.

7. Li, X.; Zhu, A. L.; Qu, W.; Wang, H.; Hui, R.; Zhang, L.; Zhang, J., Magneli Phase Ti_4O_7 Electrode for Oxygen Reduction Reaction and its Implication for Zinc-air Rechargeable Batteries. *Electrochim. Acta* **2010**, *55*, 5891-5898.
8. Page, Y. L.; Strobel, P., Structural Chemistry of Magneli Phases Ti_nO_{2n-1} ($4 \leq n \leq 9$). I. Cell and Structure Comparisons. *J. Solid State Chem.* **1982**, *43*, 314-319.
9. Page, Y. L.; Strobel, P., Structural Chemistry of Magneli Phases Ti_nO_{2n-1} , $4 \leq n \leq 9$. IV. Superstructure in Ti_4O_7 at 140 K. *J. Solid State Chem.* **1984**, *53*, 13-21.
10. Page, Y. L.; Strobel, P., Structural Chemistry of the Magneli Phases Ti_nO_{2n-1} , $4 \leq n \leq 9$. II. Refinements and Structural Discussion. *J. Solid State Chem.* **1982**, *44*, 273-281.
11. Page, Y. L.; Strobel, P., Structural Chemistry of Magneli Phases Ti_nO_{2n-1} ($4 \leq n \leq 9$). III. Valence Ordering of Titanium in Ti_6O_{11} at 130 K. *J. Solid State Chem.* **1983**, *47*, 6-15.
12. Weissmann, M.; Weht, R., Electronic and Magnetic Properties of the Different Phases of Ti_4O_7 from Density Functional Theory. *Phys. Rev. B.* **2011**, *84*, 144419.
13. Vettraiño, M.; Trudeau, M.; Lo, A. Y. H.; Schurko, R. W.; Antonelli, D., Room-Temperature Ammonia Formation from Dinitrogen on a Reduced Mesoporous Titanium Oxide Surface with Metallic Properties. *J. Am. Chem. Soc.* **2002**, *124*, 9567-9573.
14. Xu, X.; Randorn, C.; Efstathiou, P.; Irvine, J. T. S., A Red Metallic Oxide Photocatalyst. *Nature Mater.* **2012**, *11*, 595-598.
15. Tominaka, S., Topotactic Reduction Yielding Black Titanium Oxide Nanostructures as Metallic Electronic Conductors. *Inorg. Chem.* **2012**, *51*, 10136-10140.
16. Leonov, I.; Yaresko, A. N.; Antonov, V. N.; Schwingenschlgl, U.; Eyert, V.; Anisimov, V. I., Charge Order and Spin-Singlet Pair Formation in Ti_4O_7 . *J. Phys. Condens. Matter* **2006**, *18*, 10955-10964.
17. Bartholomew, R. F.; Frankl, D. R., Electrical Properties of Some Titanium Oxides. *Phys. Rev.* **1969**, *187*, 828-833.
18. Padilha, A. C. M.; Osorio-Guilln, J. M.; Rocha, A. R.; Dalpian, G. M., Ti_nO_{2n-1} Magneli Phases Studied using Density Functional Theory. *Phys. Rev. B.* **2014**, *90*, 035213.
19. Arif, A. F.; Balgis, R.; Ogi, T.; Iskandar, F.; Kinoshita, A.; Nakamura, K.; Okuyama, K., Highly Conductive Nano-sized Magneli Phases Titanium Oxide (TiO_x). *Sci. Rep.* **2017**, *7*, 3646.
20. Smith, J. R.; Walsh, F. C., Electrodes Based on Magneli Phase Titanium Oxides: the Properties and Applications of Ebonex (R) Materials. *J. Appl. Electrochem.* **1998**, *28*, 10211033.

21. Walsh, F. C.; Wills, R. G. A., The Continuing Development of Magneli Phase Titanium Suboxides and Ebonex/textregistered Electrodes. *Electrochim. Acta* **2010**, *55*, 6342-6351.
22. Portehault, D.; Maneeratana, V.; Candolfi, C.; Oeschler, N.; Veremchuk, I.; Grin, Y.; Sanchez, C.; Antonietti, M., Facile General Route toward Tunable Magneli Nanostructures and Their Use as Thermoelectric Metal Oxide/Carbon Nanocomposites. *ACS Nano* **2011**, *5*, 90529061.
23. Harada, S.; Tanaka, K.; Inui, H., Thermoelectric Properties and Crystallographic Shear Structures in Titanium Oxides of the Magneli Phases. *J. Appl. Phys.* **2010**, *108*, 083703.
24. Kundu, D.; Black, R.; Berg, E. J.; Nazar, L. F., A Highly Active Nanostructured Metallic Oxide Cathode for Aprotic Li-O₂ Batteries. *Energy Environ. Sci.* **2015**, *8*, 1292-1298.
25. Huang, S.-S.; Lin, Y.-H.; Chuang, W.; Shao, P.-S.; Chuang, C.-H.; Lee, J.-F.; Lu, M.-L.; Weng, Y.-T.; Wu, N.-L., Synthesis of High-Performance Titanium Sub-Oxides for Electrochemical Applications Using Combination of Sol–Gel and Vacuum-Carbothermic Processes. *ACS Sustain. Chem. Eng.* **2018**, *6*, 3162-3168.
26. Bousoulas, P.; Michelakaki, I.; Tsoukalas, D., Influence of Oxygen Content of Room Temperature TiO_{2-x} Deposited Films for Enhanced Resistive Switching Memory Performance. *J. Appl. Phys.* **2014**, *115*, 034516.
27. Padilha, A. C. M.; Rocha, A. R.; Dalpian, G. M., DFT+U Simulation of the Ti₄O₇-TiO₂ Interface. *Phys. Rev. Applied.* **2015**, *3*, 024009.
28. Zhou, X.; Liu, N.; Schmuki, P., Photocatalysis with TiO₂ Nanotubes: “Colorful” Reactivity and Designing Site-Specific Photocatalytic Centers into TiO₂ Nanotubes. *ACS Catal.* **2017**, *7*, 3210-3235.
29. Li, X.; Yu, J.; Low, J.; Fang, Y.; Xiao, J.; Chen, X., Engineering Heterogeneous Semiconductors for Solar Water Splitting. *J. Mater. Chem. A* **2015**, *3*, 2485-2534.
30. Yamada, Y.; Kanemitsu, Y., Determination of Electron and Hole Lifetimes of Rutile and Anatase TiO₂ Single Crystals. *Appl. Phys. Lett.* **2012**, *101*, 133907.
31. AlSalka, Y.; Hakki, A.; Schneider, J.; Bahnemann, D. W., Co-Catalyst-Free Photocatalytic Hydrogen Evolution on TiO₂: Synthesis of Optimized Photocatalyst through Statistical Material Science. *Appl. Catal. B: Environ.* **2018**, *238*, 422-433.

32. Naldoni, A.; Altomare, M.; Zoppellaro, G.; Liu, N.; Kment, Š.; Zbořil, R.; Schmuki, P., Photocatalysis with Reduced TiO₂: From Black TiO₂ to Cocatalyst-Free Hydrogen Production. *ACS Catal.* **2019**, *9*, 345-364.
33. Zhang, G.; Zou, J.; Xu, X., Reduced 3d Transition Metal Oxides Work as Solid-State Sources of Solvated Electrons and Directly Inject Electrons into Water for H₂ Production under Mild Thermal or IR Excitation. *Adv. Sustainable Syst.* **2018**, *2*, 1700139.
34. Sinhamahapatra, A.; Jeon, J.-P.; Yu, J.-S., A New Approach to Prepare Highly Active and Stable Black Titania for Visible Light-Assisted Hydrogen Production. *Energy Environ. Sci.* **2015**, *8*, 3539-3544.
35. J.Moulder; W.Stickle; P.Sobol; Bomben, K., *Handbook of X-rayphotoelectron spectroscopy*, 2nd ed. Perki- nElmer: **1992**, p44-p45.
36. Sayers, C. N.; Armstrong, N. R., X-ray Photoelectron Spectroscopy of TiO₂ and Other Titanate Electrodes and Various Standard Titanium Oxide Materials: Surface Compositional Changes of the TiO₂ Electrode during Photoelectrolysis. *Surf. Sci.* **1978**, *77*, 301-320.
37. Li, L. H.; Deng, Z. X.; Xiao, J. X.; Yang, G. W., A Metallic Metal Oxide (Ti₅O₉)-Metal Oxide (TiO₂) Nanocomposite as the Heterojunction to Enhance Visible-Light Photocatalytic Activity. *Nanotechnology* **2015**, *26*, 255705.
38. Zhou, X.; Zolnhofer, E. M.; Nguyen, N. T.; Liu, N.; Meyer, K.; Schmuki, P., Stable CoCatalyst-Free Photocatalytic H₂ Evolution from Oxidized Titanium Nitride Nanopowders. *Angew. Chem. Int. Ed.* **2015**, *54*, 13385-13389.
39. Houlihan, J. F.; Mulay, L. N., Correlation of Magnetic Susceptibility, Electrical Conductivity, and Structural Parameters of Ti₄O₇ via EPR Spectroscopy. *Phys. Stat. Sol. (b)* **1974**, *61*, 647656.
40. Zhou, X.; Hublein, V.; Liu, N.; Nguyen, N. T.; Zolnhofer, E. M.; Tsuchiya, H.; Killian, M. S.; Meyer, K.; Frey, L.; Schmuki, P., TiO₂ Nanotubes: Nitrogen-Ion Implantation at Low Dose Provides Noble-Metal-Free Photocatalytic H₂-Evolution Activity. *Angew. Chem. Int. Ed.* **2016**, *55*, 3763-3767.
41. Chen, X.; Liu, L.; Yu, P. Y.; Mao, S. S., Increasing Solar Absorption for Photocatalysis with Black Hydrogenated Titanium Dioxide Nanocrystals. *Science* **2011**, *331*, 746-750.
42. Fujishima, A.; Zhang, X.; Tryk, D. A., TiO₂ Photocatalysis and Related Surface Phenomena. *Surf. Sci. Rep.* **2008**, *63*, 515-582.
43. Liborio, L.; Mallia, G.; Harrison, N., Electronic Structure of the Ti₄O₇ Magneli Phase. *Phys.*

Table of Contents



Nanosopic Magnéli phases, formed intrinsically in anatase, can enable significant photocatalytic H₂ generation – this without the use of any extrinsic co-catalyst in anatase. Key is the metallic band of Ti₄O₇ that induces a particle internal charge separation and transfer cascade with suitable energetics and favorable dimensions that are highly effective for H₂ generation.